arXiv:1702.02987v1 [cond-mat.mes-hall] 9 Feb 2017

Modification of microstructure and micromagnetic properties in Gd-Fe thin films by rapid thermal processing

A. Talapatra[a,*], J. Arout Chelvane[b], B. Satpati[c], S. Kumar[d], J. Mohanty[a]

[a]*Nanomagnetism and Microscopy Laboratory, Department of Physics Indian Institute of Technology Hyderabad, Kandi, Sangareddy, 502285, Telangana, India*
[b]*Defence Metallurgical Research Laboratory, Hyderabad-500058, India*
[c]*Saha Institute of Nuclear Physics, HBNI, 1/AF Bidhannagar, Kolkata 700064, India*
[d]*National Centre for Compositional Characterisation of Materials, Hyderabad-500062, India*

Abstract

Impact of rapid thermal processing (RTP) on microstructure and magnetic properties of Gd-Fe thin films have been investigated with a special emphasis to magnetic microstructure. 100 nm thick amorphous Gd-Fe film shows elongated stripe domains with characteristic feature size of 122 nm, which signifies the development of perpendicular magnetic anisotropy (PMA) in this system. RTP at 550 ^oC for different time intervals *viz.* 5, 10, 15, 20 minutes induces the crystallization of Fe over the amorphous Gd-Fe matrix. Cross-sectional imaging with transmission electron microscope reveals the presence of Fe nanocrystal and the reacted film-substrate interface, which has also been verified by Rutherford backscattering spectrometry. With increasing RTP time, the characteristic size and the threshold height of the topographic feature increases. While the magnetic contrast drops down for the processed films, the increasing threshold height of the nanocrystalline grains results a topography dominated mixed phase in the magnetic force microscopy images. The magnetization measurements clearly indicate a re-orientation of the magnetization direction from perpendicular to the plane of the surface. To unravel the effect of anisotropy modification on domain structure, 3D micromagnetic simulations have been performed, which showed that with 50% reduction of original anisotropy, the magnetization tries to orient in the plane of the surface, whereas an in-plane (along xz plane) tilt angle of 30^o has been estimated to be the threshold for the decrease in perpendicular component of magnetization in the investigated Gd-Fe thin film system.

Keywords: Rare-earth Transition metal Alloy, Rapid Thermal Processing, Magnetic Domain, Tilted Anisotropy, Micromagnetic Simulation

*Corresponding author
Email addresses: ph13p1001@iith.ac.in, talapatra.abhishek@yahoo.in (A. Talapatra), jmohanty@iith.ac.in (J. Mohanty)

1. Introduction

Magnetic thin films have ushered in a new era in magnetic and magneto-optical recording technology. With the rapid research progress on magnetic materials with PMA, high density data storage (1 Tb/in^2) is being attempted. Higher magnetic anisotropy makes the system stable by getting rid of thermal fluctuation of spins. The problem associated with higher PMA is higher coercivity. This offers a new challenge for writing the media within the limited field of the existing write heads. To circumvent the problem, heat assisted magnetic recording has been investigated, where the magnetic anisotropy is tailored to be locally weak by laser heating to switch the media with a lower external magnetic field. However, the implementation of this method in a portable device is not very straight forward. So, the search for different methods of anisotropy tuning by external perturbations has gained an active interest of contemporary research.

GdFe is a very popular material system due to its interesting property of tunable PMA in amorphous as-deposited condition. It has been the centre of attraction of the research community around the globe since last few decades due to its applicability in magneto optical recording. The reason behind the evolution of PMA and reverse spin re-orientation transition (SRT) with respect to film thickness and temperature has still been debated. From the existing literature, the contribution of the magnetic dipolar interaction behind the determination of PMA can be evidenced [1]. The role of structural parameters and their correlations to the magnetic properties have been discussed there. The surface SRT in Gd films on Fe in presence of magnetic fields was elaborately explained by Camley exploiting mean field theory and atomistic model [2]. The phase transition to a twisted spin state for anti-ferromagnetically coupled Gd and Fe sublattices at higher field has also been shown by the same researcher [3, 4]. The generic sources of PMA in amorphous rare earth-transition metal (RE-TM) alloy systems has been pointed out in the light of fundamental electromagnetic theory [5]. The experimental studies confirm that the sources are material specific and vary with deposition process parameters [6]. From the point of view of application in magneto-optical recording with different RE-TM alloys, an excellent review has been provided by Mieklejohn [7], followed by Hansen *et al.* on magneto-optical properties of Gd, Tb, Fe, Co based binary RE-TM alloys [8].

The purview to the domain imaging in Gd-Fe alloy or in Gd/Fe multilayer system started to a great extent in the beginning of 21st century. The high resolution domain imaging techniques along with the study of material sensitive magnetic properties have been developed with high intensity synchrotron X-ray. Emüller *et al.* utilized magnetic transmission x-ray microscopy technique with x-ray magnetic circular dichroism for the quantitative domain analysis in perpendicularly magnetized Gd/Fe multilayer [9]. A considerable piece of research has been performed by Miguel and colleagues for the development of X-ray resonant magnetic scattering to study the domain structure and their dynamics for Gd-Fe thin films [10, 11]. Utilizing the soft ferrimagnetic nature of GdFe, detailed study of exchange bias at the soft-hard ferrimagnetic interfaces has been carried out by Mangin et al. [12, 13]. In the most recent scenario, the RE-TM alloy thin films have gained interest in the field of studies of ultrafast magnetization dynamics due to the different temporal response of

the respective sub-lattices [14]. Gd/Fe multilayer system has also been used for advanced dichroic coherent imaging technique [15].

On the basis of the aforesaid existing research, we found that a systematic study on anisotropy tuning in Gd-Fe thin films has not been attempted yet. Konings *et al.* showed the anisotropy engineering in Gd-Fe thin films by locking the domains into the pinning cites, created by focused ion beam patterning [16]. But, the correlation with the structural properties seems to be missing. However, tailoring of magnetic anisotropy in TbFeCo thin films by rapid thermal annealing has been reported by Umadevi et al. [17]. Lack of information on the magnetic microstructure and its correlation with the magnetic properties paved the motivation of our study. Here, we report the impact of RTP on structural, micro-structural and magnetic properties of Gd-Fe thin films with a special emphasis towards magnetic microstructure. To overcome the experimental limitations, 3D-micromagnetic simulation has been performed to observe the consequences of anisotropy tilt in magnetic domains.

2. Experimental Detail

100 nm thick Gd-Fe films were deposited by electron beam evaporation at room temperature on Si $< 100 >$ substrates under background pressure of 2×10^{-6} Torr. The deposition rate was optimized to be 2 $\mathring{A}/s$ employing an alloy target with composition $Gd_{50}Fe_{50}$. The substrate has been rotated with a constant speed of 10 rpm to ensure uniformity in deposition. A 3 nm thick capping layer of Cr was used to protect the films from oxidation. The thickness values mentioned here are recorded from the quartz crystal monitor associated to deposition unit. RTP experiments have been performed at 550 ^oC under high vacuum for different annealing times *viz.*, 5, 10, 15, 20 minutes (min) with a RTP furnace, where the ramp rate of heating was optimized at 250 $^oC/min$. The structural information was obtained by grazing incidence x-ray diffraction (GI-XRD) using Cu K_α radiation at an angle of incidence 1^o. The microstructure of the films has been characterized by cross-sectional transmission electron microscope (XTEM), high-angle annular dark-field scanning transmission electron microscopy (HAADF-STEM), energy dispersive x-ray spectroscopy (EDS), using FEI, Tecnai G2 F30, S-Twin microscope operating at 300 kV. Field emission scanning electron microscope (FESEM) equipped with EDS was used to study the surface morphology along with the overall composition. The composition was further checked by Rutherford backscattered spectroscopy (RBS) technique using carbon (^{12}C) beam of energy 6991 keV, derived from 3 MV tandetron accelerator (HVEE, Europa). The scattering angle was set at 170^o and passive implanted planar Silicon (PIPS) detector was utilized to carry out the experiment in a vacuum level of 5×10^{-6} Torr inside the sample chamber. The room temperature magnetization measurements have been carried out with vibrating sample magnetometer (VSM). Atomic force microscopy (AFM) and magnetic force microscopy (MFM) were performed simultaneously by using CoCr coated antimony doped Si tip at room temperature without any external magnetic field.

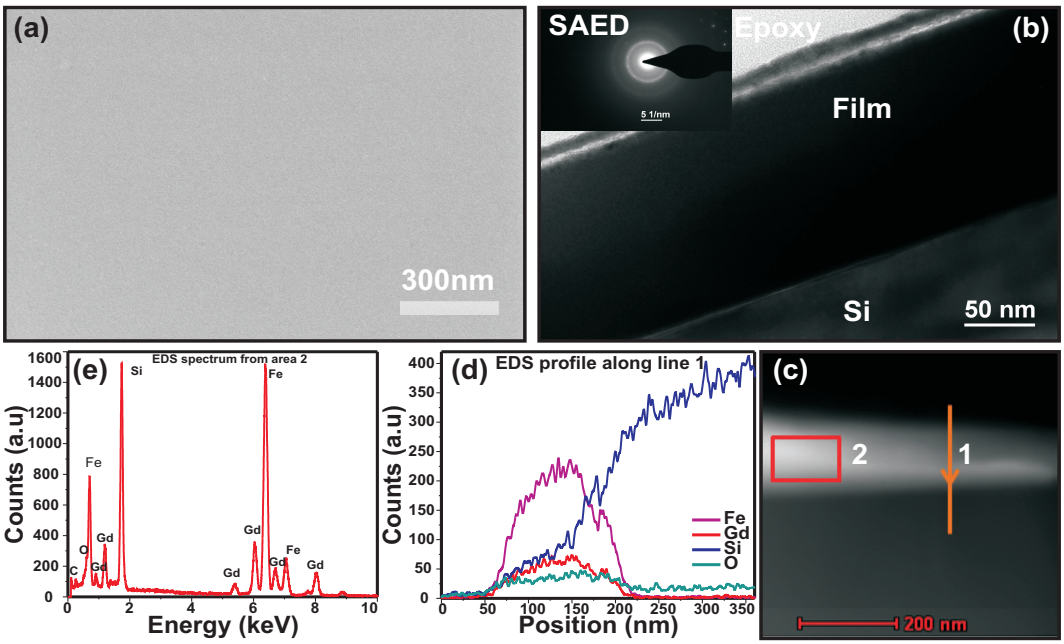

Figure 1: (a) FESEM image, (b) XTEM image with SAED pattern as inset for as-prepared Gd-Fe thin film, (c) STEM-HAADF image, (d) EDS line profile along line 1 in (c) and (e) EDS spectrum from area 2 in (c).

3. Results and Discussions

The e-beam evaporated 100 nm thick Gd-Fe film shows a smooth surface with no identifiable features as in Fig. 1(a). The overall composition (atomic %) of the film has been found to be $Gd_{16.6}Fe_{83.4}$ employing EDS, associated with FESEM. This has been checked at different places of the films and seen to be similar which ensures the homogeneity in composition for the films. The amorphous nature of the as-prepared film has been confirmed by the selected area electron diffraction (SAED) pattern, taken along the cross-section, as shown in Fig. 1(b). The film-substrate interface is very sharp, devoid of any diffusion or intermixing. The EDS line profile has been shown in Fig. 1(d), obtained across line 1 in the cross-sectional STEM-HAADF image (Fig. 1(c)) and the elemental composition is estimated to be $Gd_{13.7}Fe_{86.3}$. The EDS spectrum from area 2 (in Fig. 1(c)) has also been depicted in Fig. 1(e). No other source of contamination has been evidenced from the EDS spectrum, except the presence of oxygen. For the as-prepared sample, the presence of oxygen has been observed with increasing time, but the magnetic property does not change considerably.

Fig. 2(a) and (b) exhibits respectively the AFM and MFM images of the as-prepared sample, which shows that the magnetic phase is free from topographic influences. MFM reveals elongated, periodic stripe domain pattern with high magnetic phase contrast. The domains are essentially the self organization of magnetization into alternating up-down magnetized bands. They are formed due to the competition between the exchange and anisotropy energies which favor a single domain state with magnetization perpendicular to the film plane, with long ranged demagnetizing field that favors the creation of in-plane (IP) domain walls by breaking the system into multi-domain state. The domain periodicity has been calculated

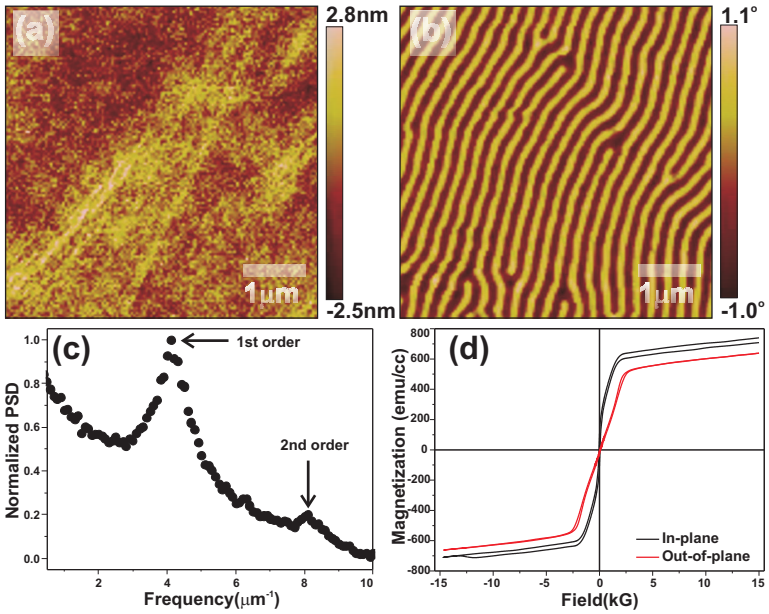

Figure 2: (a) AFM, (b) MFM, (c) PSD profile of the MFM image and (d) hysteresis loop along IP and OOP direction for 100 nm thick as-prepared Gd-Fe thin film.

from the 2D isotropic power spectral density (PSD) profile as in Fig. 2(c), estimated from the Fourier transform of the MFM image. This allows us to obtain the periodic distribution of the MFM image (twice the domain size) and their relative weight [18]. The peak of the PSD curve points out the wavelength of the most predominant feature in the image [19]. The PSD is fitted with a Lorentzian to point out the mean value and standard deviation which account for the domain periodicity and the associated error bar respectively. The domain size turned out to be around 122 (± 2) nm by inverting the frequency of the 1st order peak. The presence of the other lower order peak designates the long range domain ordering. Similar kind of domains in as-prepared Gd-Fe films has also been reported [10]. But, the magnetic properties are very sensitive to the processing conditions [20, 21] such as temperature, pressure, deposition time and internal stress as well. We have reported the domain evolution as a function of film thickness for identical system [22]. This kind of sub-200 nm sized domains are usually the signature of the development of PMA in thin films and results in a slanted hysteresis loop with almost zero remanence when measured along the out-of-plane (OOP) direction, as shown in Fig. 2(d). Similar feature of domains and hysteresis loop has also been reported for Co/Pt multilayer [23, 24] and also in Gd-Fe thin films [16]. While the coercivity for the IP (51 Gauss) and OOP (43 Gauss) loops are comparable, the remanence is more for the IP loop as observed from Fig. 1(d).

As our interest involves anisotropy tuning in Gd-Fe thin films, so we have performed RTP at 550 ^oC for different time intervals which results a global change in material properties, unlike local modifications by laser [25, 23] or focused ion beam irradiation [26, 16]. While the as-prepared film shows amorphous nature, RTP induces crystallinity in the films, degree of which increases upon increasing processing time, as observed from Fig. 3. The appearance

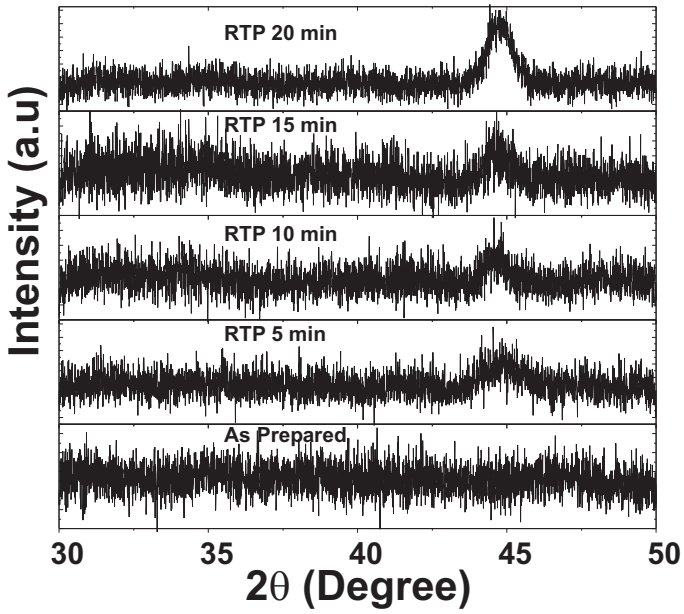

Figure 3: XRD results for as-prepared film and films after RTP at 550 ^oC with different time interval (mentioned in respective places).

of the peak at $2\theta \sim 44.67^o$ corresponds to the highest intensity peak of Fe from (110) plane (JCPDS card number: 00-006-0696). This designates the nucleation of crystalline Fe over the amorphous Gd-Fe matrix. Further, this has been verified by XTEM images, performed on the samples after RTP of 20 min (Fig. 4(a)). A clear indication about the presence of Fe can be observed from the EDS line profile (Fig. 4(f)) of the cross-sectional STEM-HAADF image in Fig. 4(e), mostly near the top and bottom surfaces. The composition is estimated to be $Gd_{15.4}Fe_{84.6}$ along the depth. The top surface is rough due to the nm-sized crystalline growth of iron, which is evident from the selected area electron diffraction (SAED) pattern (inset of Fig. 4(a)). The d-spacings calculated from the diameter of the rings match with the reflections of bcc Fe phase and the presence of spots confirms that the Fe nanocrystals are distributed over the amorphous phase of Gd-Fe. Further, one of the crystalline Fe particle at the top surface has been shown in the HRTEM image of Fig. 4(b). The lattice spacing estimated to be 2.03 Å from the IFFT image of the selected area as in Fig. 4(b). This matches with [110] inter planar spacing of bcc Fe with lattice constant of 2.867Å. As RTP is a non-equilibrium process with very high ramp rate of heating, so the crystallization of Fe is expected to be favorable due to its smaller atomic radius compared to Gd. Besides, the XTEM image in Fig. 4(a) also confirms the presence of Fe nanocrystal at the reacted film-substrate interface. Similar observation of the crystallization of FeCo alloy over amorphous TbFeCo matrix has been reported in [17]. On top of that, elemental mapping (shown in Fig. 4(i))has been performed using STEM-HAADF-EDS technique along the area shown in Fig. 4(h). This essentially verifies the presence of Fe and Gd over the considered area.

While the as-prepared film shows a feature-less smooth surface (Fig. 1(a)), the presence of island-like granular microstructure has been evidenced in the surface FESEM micrographs

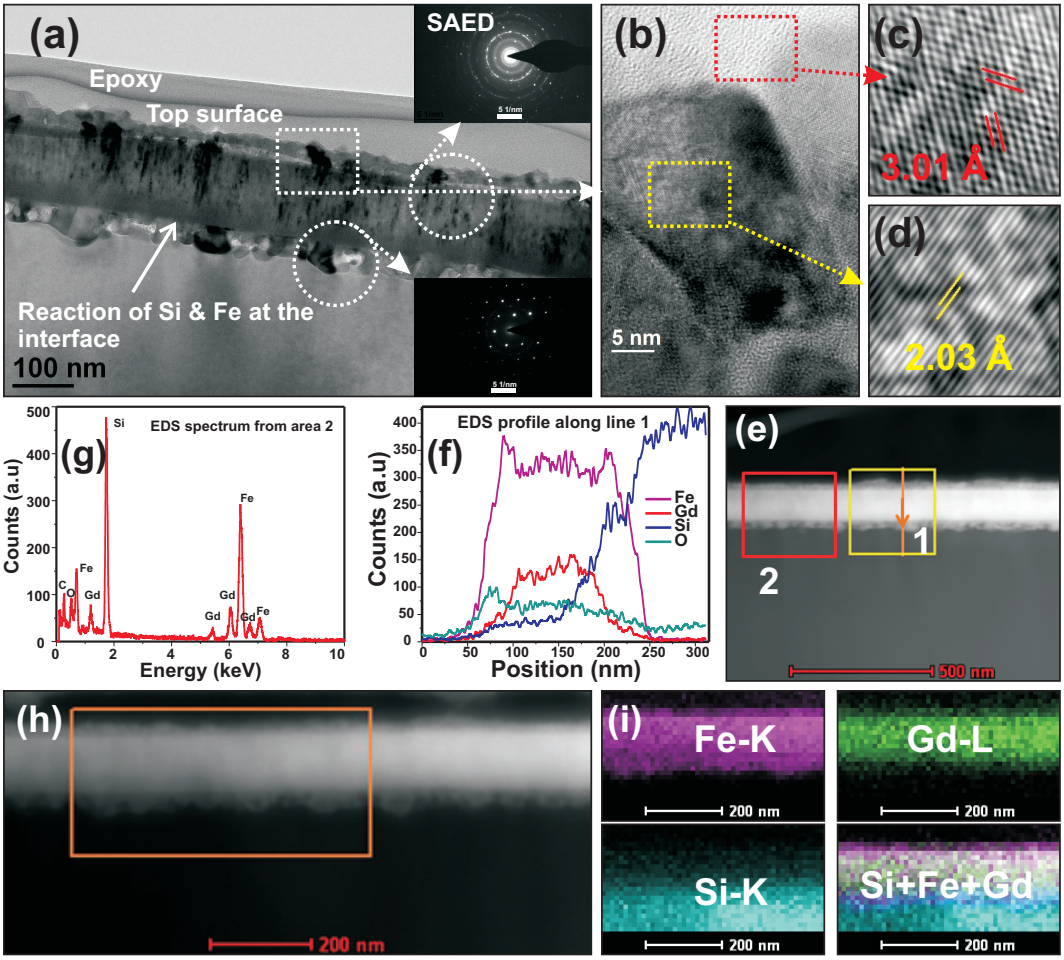

Figure 4: (a) Cross-sectional TEM image for Gd-Fe thin film after RTP of 20 min, inset shows the SAED patterns taken from the top surface and at the film-substrate interface, (b) high resolution TEM image of the selected area from (a), (c) and (d) represent area specific IFFT images showing lattice fringes, (e) STEM-HAADF image, (f) EDS profile along line 1 in (c), (g) EDS spectrum from area 2 in (c), (h) STEM-HAADF image with (i) elemental mapping in the selected region.

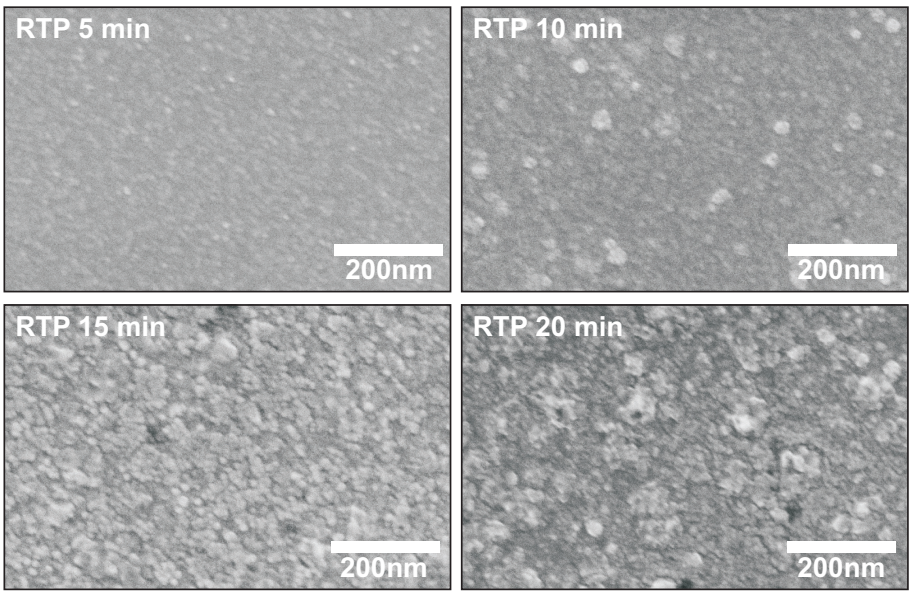

Figure 5: FESEM surface micrographs for Gd-Fe films with different RTP time, mentioned in the top left corner of the images.

over a large field of view, as shown in Fig. 5. It can be qualitatively observed that the distribution of the grains in the surface is irregular and the grain size increases with the increase in RTP time. At 20 min RTP time, the size becomes maximum with highest irregularity in the distribution. The measurement of the overall composition by EDS, performed for the RTP samples showed a very little increment of the rare-earth metal upon increasing the RTP time and this is listed in Table 1.

Further study of composition has been carried out with RBS technique which provides higher resolution compared to EDS. The experimental and the simulated RBS data along with the simulation model has been shown in Fig. 6. The overall composition for the as-prepared film has been estimated to be $Gd_{16.6}Fe_{83.6}$, from the area under the experimental curve in Fig. 6(a). This turned out to be very similar with the EDS data. For depth profiling of the elemental composition, the experimental data has been simulated with various model having different layer compositions. The best fitted model for the as-prepared film has been shown in Fig. 6(c), which shows inhomogeneous distribution of Gd and Fe throughout the depth of the film by considering five intermediate layers. Now the complexity arises after performing RTP for 10 min and the data is shown in Fig. 6(b). The composition calculated from the area under the curve is again comparable to the EDS data, mentioned in Table 1. But the best-fit model shows us the real picture of the RTP effect by considering ten intermediate layers. It seems that the Cr capping layer has been oxidized and presence of Fe can be evidenced in the top and bottom layers, whereas for the middle layers, the presence of Gd-Fe alloy is observed. Apart from that, the diffusion of Si into the film may lead to the formation of alloy of Fe and Si at the film-substrate interface, which is evident from Fig. 6(d). The results of RBS experiments also match with the findings of XTEM, where we get an extra information on the crystalline state of Fe at the top and bottom

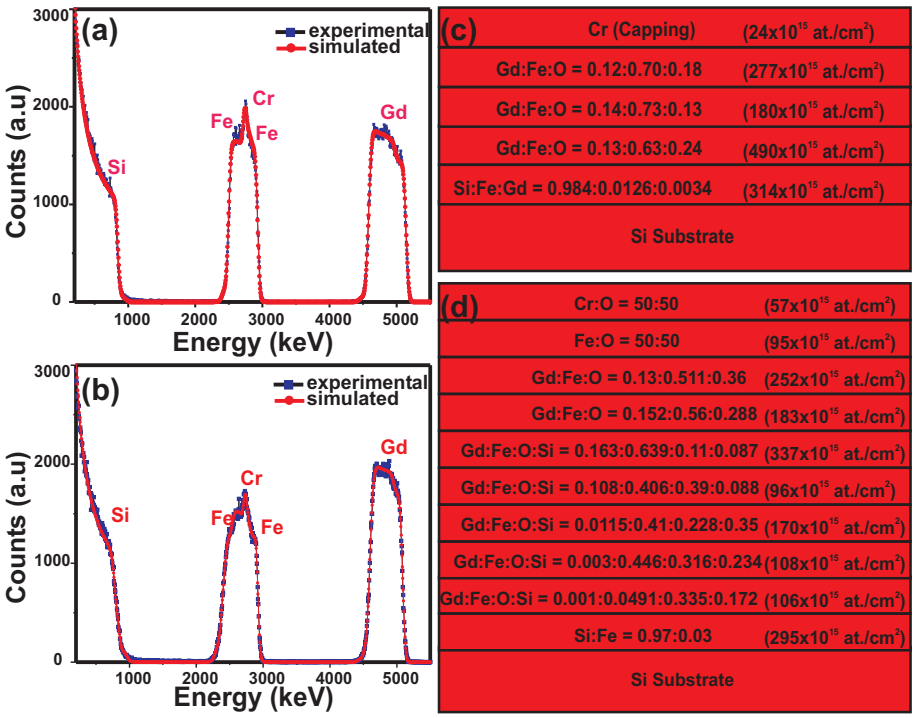

Figure 6: Experimental and simulated data for (a) as-prepared and (b) the processed sample for 10 min, (c) and (d) are the model considered for simulation in the case of (a) and (b) respectively.

surfaces.

To probe the topography microscopically with higher resolution, AFM measurement has been carried out for all the samples, which is shown in the series of Fig. 7(a). Similar findings of increasing nanocrystalline grain growth has also been noticed with increasing RTP time. To get quantitative information from the AFM images, roughness, grain diameter and most probable threshold height of the topographic feature have been estimated and mentioned in Table 1. It has been observed that the surface roughness increases monotonically with RTP time and reaches almost 4.25 times when the RTP is performed for 20 min compared to that for 5 min. Due to the increasing RTP time, the crystalline grain diameter increases, but the size distribution gets broader (as the error is very high) for 20 min sample. This can be attributed to the increase in non-uniformity in the distribution of the crystallites over the film surface which has also been qualitatively understood from the FESEM images (Fig. 5). From the point of view of scanning probe microscopy, threshold height is an important criterion which designates the average height of the topographic feature with respect to the maximum height in the depth histogram analysis. The most probable threshold height turns out to be maximum for the sample with processing time of 15 min and again drops down at 20 min. But comparatively higher value of the full width half maxima (FWHM) essentially proves again the non-uniform growth of the crystallites for the films with RTP time of 20 min.

Magnetic microstructure of the films has been imaged using a magnetized tip with a

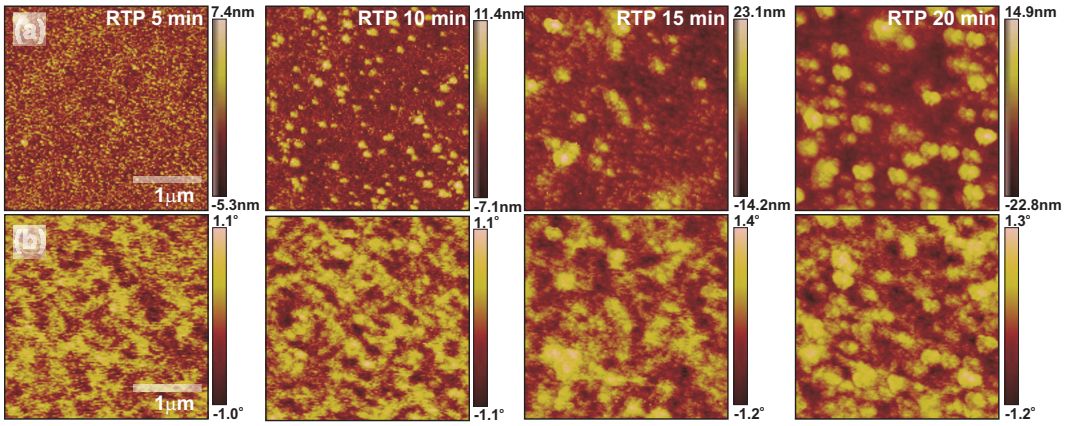

Figure 7: (a) AFM and (b) MFM images of the samples, processed with different RTP time, mentioned in the top right corner of the respective images. The area of scanning for AFM and MFM are same (vertically). The scale bar is same for all the images.

Table 1: Variation of overall elemental composition, roughness, grain size and threshold height of grains with RTP time interval.

Sample Status	Composition (atomic %)	Roughness (nm)	Grain size (± error) (nm)	Most probable threshold height (± FWHM) (nm)
RTP 5 min	$Gd_{16.9}Fe_{83.1}$	1.96	140.38 (21.6)	21.27 (3.16)
RTP 10 min	$Gd_{17.2}Fe_{82.8}$	2.54	138.41 (34.3)	43.26 (3.35)
RTP 15 min	$Gd_{18.1}Fe_{81.9}$	4.84	173.5 (74.4)	107.23 (7.18)
RTP 20 min	$Gd_{18.1}Fe_{81.9}$	8.33	289 (205.8)	49.85 (15.06)

lift height of 50 nm from the sample surface and the images are shown in Fig. 7(b). The area of scanning for the AFM and MFM images are same which helps to correlate the magnetic microstructure with the topographic feature. While the as-prepared sample shows elongated stripe domains (Fig. 2(b)), the film with processing time of 5 min does not show any identifiable domain pattern. Two different magnetic contrast appear in the form of irregular patches which essentially means that the PMA of the sample gets weaker and the formation of stripe domain is no longer energetically favorable. This may take place due to the modification of magnetic anisotropy axis after the thermal processing. So, the magnetic phase contrast is expected to be weaker for the films with higher RTP time. We are unable to visualize this from the MFM image because the topographic feature dominates the magnetic phase. Starting from the sample with RTP time of 10 min, the most probable threshold height of the crystallites (Table 1) becomes comparable to the lift height of the MFM tip. As a result, short ranged Van der Waals force wins over the magnetic force and topography dominated mixed phase is obtained. MFM has also been performed with higher lift heights (not shown here), but the weaker magnetic signal results noise in the image.

Fig. 8 represents the hysteresis loops for the RTP samples measured in IP and OOP geometry. The extracted magnetic properties are summarized in Table 2. It can be observed

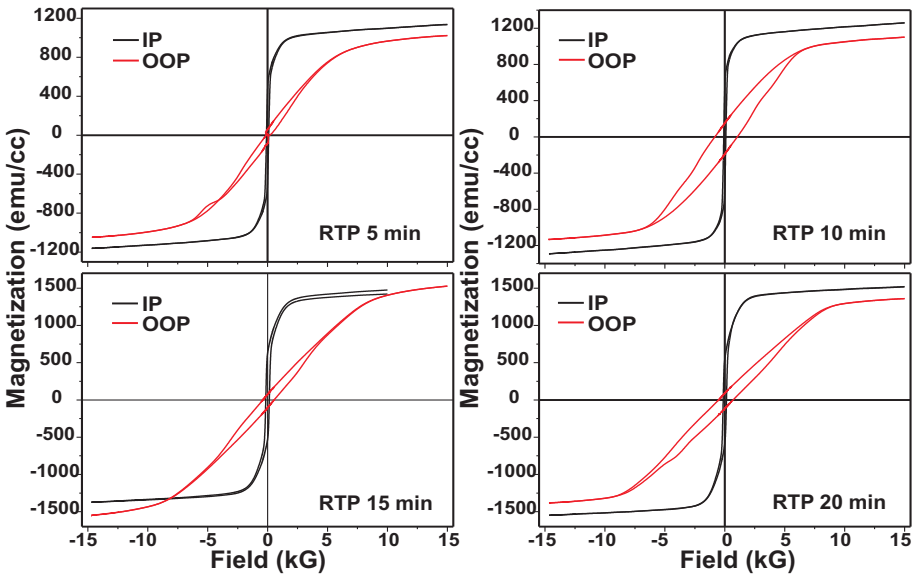

Figure 8: In-plane and out-of-plane hysteresis loops for the samples, processed with different RTP time, mentioned in the right bottom corner of the respective images.

that the remanence and saturation magnetization shows increasing trend with increasing RTP time for both the IP and OOP mode. But the specific value of the IP remanence is much greater than that in OOP mode. The increase in squareness (ratio of remanence to saturation magnetization) for the IP loops with RTP time suggests that RTP favors the magnetization to lie in the plane of the sample surface, unlike in the case of the as-prepared sample. Umadevi *et al.* [17] calculated the tilt angle of hard TbFeCo with increasing annealing time by using a formula mentioned in [27], as the cosine inverse of the ratio of the remanent magnetization for the RTP sample to that of the as-prepared sample. This calculation may show some meaningful result for the case of materials with strong PMA as in the case of TbFeCo, where the as-prepared sample shows almost square hysteresis loop. Gd-Fe being a soft magnetic material with weak PMA, the way of calculation of tilt angle by similar method does not hold good. Here we need to understand the anisotropy modification in terms of increase in IP remanence and squareness compared to the OOP mode. On top of that, the OOP saturation field is almost 3 times the IP saturation field, which indicates that the IP direction becomes the preferential orientation of magnetization after RTP. This is attributed to the Fe crystallization in the amorphous Gd-Fe phase, which applies an IP torque to the magnetic moment. However, the coercivity value observed to be more in the OOP mode and varies somewhat randomly which can be corroborated to the increase in pinning sites along vertical direction due to the higher threshold heights of the nanocrystallites.

In the light of the magnetic microstructure and magnetization measurements, it is evident that the magnetic anisotropy is getting modified due to RTP. But the experimental limitation hindered us to image the domain structure without topographic influence. This has been complemented by 3D micromagnetic simulation, which directly shows the varia-

Table 2: Variation of IP and OOP Remanence (M_R), coercivity (H_c), saturation magnetization (M_s) and saturation field (H_s) with RTP time interval.

Sample Status	M_R IP (OOP) (emu/cc)	H_c IP (OOP) (Gauss)	M_s IP (OOP) (emu/cc)	H_s IP (OOP) (Gauss)
RTP 5 min	462.8 (70.7)	97.4 (118)	1007 (862.5)	2138 (6585)
RTP 10 min	559 (171)	92.2 (938.4)	1138 (1001.8)	3283 (7445)
RTP 15 min	579 (89)	152.4 (474.4)	1260 (1404)	3292 (9988)
RTP 20 min	562 (102.7)	146 (609)	1414 (1293.4)	3345 (10020)

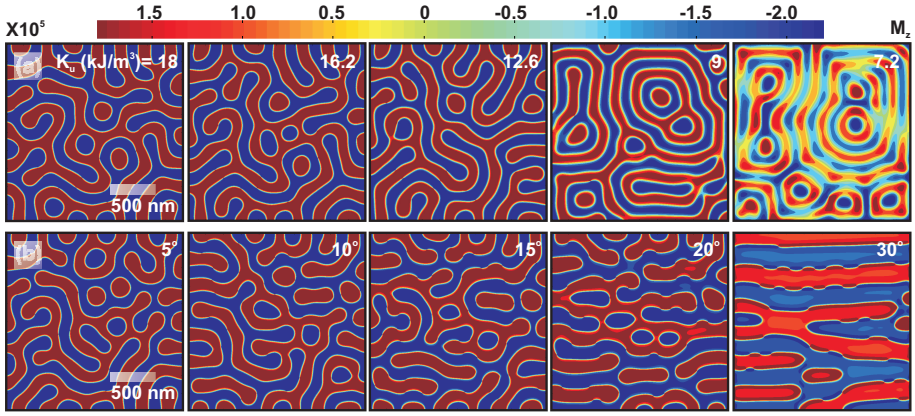

Figure 9: Simulated domain images with (a) anisotropy reduction and (b) with IP tilt along xz plane. The anisotropy value (in kJ/m^3) and the value of the tilt angle (in degree) has been mentioned at the top right corner of the respective images in the series of (a) and (b) respectively. The scale bar and color bar is same for all the images.

tion of magnetic domains as a function of anisotropy value as well as its IP tilt along the xz plane. The simulations of magnetic domains are carried out by OOMMF software [28] which performs the minimization of the total magnetic energy of the system, starting from a random state with uniform vertical ($+Z$) magnetization. The input parameters used for the simulations have been taken from [10] which include saturation magnetization (M_s) = 221 kA/m, uniaxial magnetic anisotropy constant (K_u) = 18 kJ/m^3 and the exchange stiffness constant (A) = 2.6 pJ/m. The volume of each cell is taken to be (4 nm)^3, which is smaller than the exchange length ($\sqrt{2A/\mu_0.M_s^2} \sim 9$ nm) of the material. The effect of finite temperature has not been considered in the simulations.

The first image of Fig. 9(a) shows the domain structure (M_z component of the magnetization vector) for a 100 nm thick Gd-Fe films, specified by the mentioned input parameters. The two different contrasts (red and blue) in the image represent oppositely magnetized alternating up-down domains having magnetization parallel or anti-parallel to the surface normal. The total area of simulation ($2\mu m \times 2\mu m$) is much greater than the characteristic feature of the domains, so the effect of truncation can be neglected. The domain in the first image of Fig. 9(a) shows a perfect demagnetized state with connected stripes and that can be considered to be comparable to the domain pattern of the as-prepared sample as

in Fig. 2(b). Line scans over the different areas of the domains show the average domain size to be 107 (± 5) nm, which is comparable to the domain size obtained from the experiment. On top of that, the domain wall ($\sqrt{M_x^2 + M_y^2}$ component) width turned out to be 26 (± 2) nm which matches very close to the theoretical value of 28 nm ($\pi.\sqrt{A/K_u}$). In order to study the effect of anisotropy in OOP to IP transition of the magnetization, we have systematically decreased the anisotropy value at an interval of 10% of the original value, mentioned above. The variation of domain size and domain wall width as a function of anisotropy value has been depicted in Fig. 10(a). The simulated domain size decreases with decreasing the anisotropy value and simultaneously the domain wall width increases. Finally, at $K_u = 9\ kJ/m^3$ (50% less compared to the original), IP components come into the picture and as a result of that the elongated stripe pattern tries to shrink to a closed circular-like domains to minimize the magnetostatic energy. The comparable values of domain size and domain wall width at the same anisotropy value (Fig. 10(a)) also signifies a strong competition between the IP and OOP components of the magnetization. Similar observations on domain pattern were also reported for Co/Pt multilayer in response to ultrafast laser pulse and was also verified by micromagnetic simulations [23]. The series of images in Fig. 9(b) shows the effect of anisotropy tilt along the xz plane. The first image in Fig. 9(b) series shows the domain configuration at 5 ^{o} tilt angle with respect to the original one, as in the first image of Fig. 9(a). With increasing tilt angle, the domain structure is getting modified and the random stripe domain pattern is converted to irregular discrete bubbles and patches, trying to orient along the longitudinal direction. This effect is very clear from the domain image with a tilt angle of 20^o onwards. Moreover, the contrast variation in the normalized images confirms that the PMA decreases and the resulting anisotropy does not energetically favor the formation of elongated periodic stripe pattern which has also been evidenced from the experimental results. While the irregular domain pattern with different color contrast hinders to estimate the domain size properly, the energetics of the system (Fig. 10(b)) clearly throw light towards the micromagnetic phenomena. The monotonic decrease in total energy of the system is followed by the decrease in other magnetic energies, namely uniaxial anisotropy energy (E_{Ku}), exchange energy (E_A) and demagnetization energy (E_D) with increasing tilt angle. But the maximum variation of E_{Ku} is calculated to be 75% whereas the other two energies show a negligible variation up to the tilt angle of 30^o. This may be considered as the threshold value of the tilt angle in this material system to offer a spin re-orientation after which IP component of magnetization becomes stronger. As a result, the E_A and E_D drops down to 84% and 62% respectively. Thus, our simulation results correlate the effect of magnetization tilt in magnetic microstructure as well as the energetics of the system.

4. Conclusion

Detailed study on structure, microstructure and magnetic properties have been performed on Gd-Fe thin films, subjected to RTP at different time interval. 100 nm thick amorphous as-deposited film shows elongated stripe domains with higher magnetic phase contrast which symbolizes the development of PMA in the material. RTP treatment at

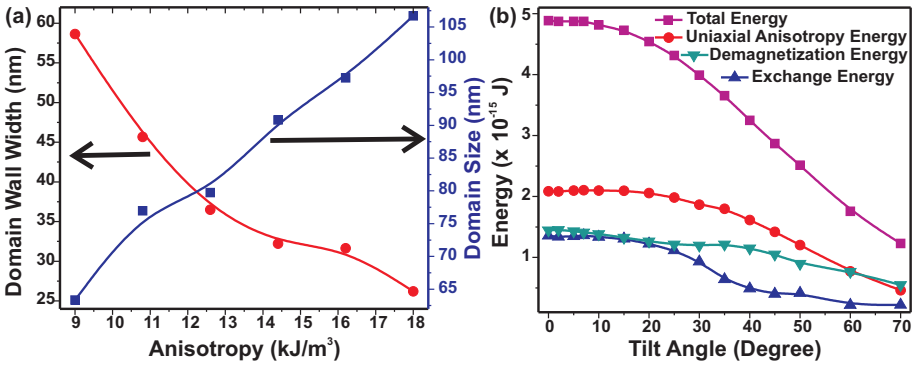

Figure 10: Variation of (a) domain size and domain wall width as a function of anisotropy value, (b) different micromagnetic energy terms along with total energy as a function of anisotropy tilt angle.

550 ^oC for different time intervals induce the nucleation of Fe nanocrystals over amorphous Gd-Fe matrix. The detailed structural study by XTEM reveals the presence of nanocrystalline iron in the top and bottom surfaces, quantification of which has been provided by RBS. FESEM surface micrographs and AFM show the irregular distribution of island-like grains on the surface, characteristic size of which increases with increasing annealing time. The magnetization studies explain that the films behave to be magnetized in the plane of the surface upon different time interval of RTP, which can be corroborated to the crystallization of Fe, that gives an IP tilt to the magnetic moment. Special thrust has been given to understand the magnetic microstructure with the increase in annealing time. The decrease in magnetic contrast and simultaneous growth of topographic feature limit us to get a topography free magnetic contrast by MFM. To unravel the modification of domain structure, 3D micromagnetic simulations have been carried out which successfully explains the change in the domain pattern, their size, orientation and micromagnetic energetics of the system under the modification of anisotropy value and its direction.

Acknowledgment

The complete work has been carried out under the scope of the project, titled DMRL/O/CARS-17, issued by DRDO, India. A. T and J. M are thankful to the Director, DMRL Hyderabad for allowing the access to the experimental facilities. Mr. Binoy Krishna Hazra is thanked for the FESEM measurements.

References

[1] T. Mizoguchi and G. S. Cargill, J. Appl. Phys. **50**, 3570 (1979)
[2] R. E. Camley, Phys. Rev. B **35 (7)**, 3608 (1987)
[3] R. E. Camley, Phys. Rev. B **37 (7)**, 3413 (1988)
[4] R. E. Camley, Phys. Rev. B **39 (16)**, 12316 (1989)
[5] H. Fu, M. Mansuripur and P. Meystre, Phys. Rev. Lett. **66 (8)**, 1086 (1991)
[6] R. J. Gambino and J. J. Cuomo, J. Vac. Sci. Tech. **15**, 296 (1978)
[7] W. H. Meiklejohn, Proc. IEEE **74 (11)**, 1570 (1986)

[8] P. Hansen, C. Clausen, G. Much, M. Rosenkranz and K. Witter, J. Appl. Phys. **66**, 756 (1989)
[9] T. Eimüller, R. Kalchgruber, P. Fischer, G. Schütz, P. Guttmann, G. Schmahl, M. Köhler, K. Prügl, M. Scholz, F. Bammes and G. Bayreuther, J. Appl. Phys. **87 (9)**, 6478 (2000)
[10] J. Miguel, J. F. Peters, O. M. Toulemonde, S. S. Dhesi, N. B. Brookes and J. B. Goedkoop, Phys. Rev. B **74**, 094437 (2006)
[11] J. Miguel, Ph.D thesis, "Static and dynamic X-ray resonant magnetic scattering studies on magnetic domains", University of Amsterdam (2005), https://iop.fnwi.uva.nl/cmp//scientific_output/phd_theses.html
[12] S. Mangin, F. Montaigne and A. Schuhl, Phys. Rev. B **68**, 140404(R) (2003)
[13] S. Mangin, T. Hauet, Y. Henry, F. Montaigne and E. E. Fullerton, Phys. Rev. B **74**, 024414 (2006)
[14] I. Radu, C. Stamm, A. Eschenlohr, F. Radu, R. Abrudan, K. Vahaplar, T. Kachel, N. Pontius, R. Mitzner, K. Holldack, A. Föhlisch, T. A. Ostler, J. H. Mentink, R. F. L. Evans, R. W. Chantrell, A. Sukamoto, A. Itoh, A. Kirilyuk, A. V. Kimel and T. Raising, Spin **5(3)**, 1550004 (2015).
[15] A. Tripathi, J. Mohanty, S. H. Dietze, O. G. Shpyrko, E. Shipton, E. E. Fullerton, S. S. Kim and I. Mcnulty, Proc. Nat. Acad. Sci. **108 (33)**, 13393 (2011)
[16] S. Konings, J. Miguel, J. Luigjes, H. Schlatter, H. Luigjes, J. Goedkoop and V. Gadgil, J. Appl. Phys. **98**, 054306 (2005)
[17] K. Umadevi, S. Bysakh, J. Arout Chelvane, S. V. Kamat and V. Jayalakshmi, J. Alloy. Comp. **663**, 430 (2016)
[18] V. Baltz, A. Marty, B. Rodmacq and B. Dieny, Phys. Rev. B **75**, 014406 (2007)
[19] S. R. Bakaul, W. Lin and T. Wu, Appl. Phys. Lett. **99**, 042503 (2011)
[20] H. Basumatary, J. Arout Chelvane, D. V. Sridhar Rao, S. V. Kamat and R. Ranjan, Thin Sol. Film. **583**, 1 (2015)
[21] K. Umadevi, J. Arout Chelvane, H. Basumatary, M. Ramudu, S. V. Kamat and V. Jayalakshmi, J. Magn. Magn. Mater. **418**, 163 (2016)
[22] A. Talapatra, J. Arout Chelvane and J. Mohanty, AIP Conf. Proc. (Accepted)
[23] A. Talapatra and J. Mohanty, J. Magn. Magn. Mater. **418**, 224 (2016)
[24] A. Talapatra and J. Mohanty, AIP Conf. Proc. **1731**, 130027 (2016)
[25] C-H. Lambert, S. Mangin, B. S. D. Ch. S. Varaprasad, Y. K. Takahashi, M. Hehn, M. Cinchetti, G. Malinowski, K. Hono, Y. Fainman, M. Aeschlimann and E. E. Fullerton, Science **345**, 1337 (2014)
[26] A. Maziewski, P. Mazalski, Z. Kurant, M. O. Liedke, J. McCord, J. Fassbender, J. Ferré, A. Mougin, A. Wawro, L. T. Baczewski, A. Rogalev, F. Wilhelm and T. Gemming, Phys. Rev. B **85**, 054427 (2012)
[27] S. Chung, S. M. Mohseni, V. Fallahi, T. N. Anh Nguyen, N. Benatmane, R. K. Dumas and J. Åkerman, J. Phys. D: Appl. Phys. **46**, 125004 (2013)
[28] M. Donahue, D. G. Porter, OOMMF user's guide, version 1.0, Intergency Report NISTIR 6376, Nat. Inst. of Standard and Tech. Gaithersburg, MD, http://math.nist.gov/oommf.